Ethyl Acetoacetate and Acetylacetone Appended Hexabromo Porphyrins: Synthesis, Spectral, Electrochemical, and Femtosecond Third-Order Nonlinear Optical Studies

Renu Kumari Rohal [a], Dipanjan Banerjee [b], Tavleen Manchanda [a], Varusha Bhardwaj,[a]

Venugopal Rao Soma*[b] and Muniappan Sankar *[a]

[a]Department of Chemistry, Indian Institute of Technology Roorkee, Roorkee 247667, India.

[b]Advanced Centre of Research in High Energy Materials (ACRHEM),
University of Hyderabad, Hyderabad 500046, Telangana, India.

Corresponding authors' e-mail addresses: soma_venu@uohyd.ac.in (V.R. Soma),
m.sankar@cy.iitr.ac.in (M. Sankar)

Table of contents

Figure S8. The ^{13} C NMR spectrum of NiTPP[EAA]Br_6 (**1-Ni**) in $CDCl_3$ at 298 K.

Figure S9. The MALDI-TOF-MS of H_2TPP[EAA]Br_6 (**1-H_2**) in positive ion mode using HABA as matrix at 298 K.

Figure S10. The MALDI-TOF-MS of CuTPP[EAA]Br_6 (**1-Cu**) in positive ion mode using HABA as matrix at 298 K.

Figure S11. The MALDI-TOF-MS of NiTPP[EAA]Br_6 (**1-Ni**) in positive ion mode using HABA as matrix at 298 K.

Figure S12. The MALDI-TOF-MS of H_2TPP[acac]Br_6 (**2-H_2**) in positive ion mode using HABA as matrix at 298 K.

Figure S13. The MALDI-TOF-MS of CuTPP[acac]Br_6 (**2-Cu**) in positive ion mode using HABA as matrix at 298 K.

Figure S14. The MALDI-TOF-MS of NiTPP[acac]Br_6 (**2-Ni**) in positive ion mode using HABA as matrix at 298 K.

Figure S15. The IR of H_2TPP[EAA]Br_6 (**1-H_2**) using KBr pellet at 298 K.

Figure S16. The IR of H_2TPP[acac]Br_6 (**2-H_2**) using KBr pellet at 298 K.

Figure S17. The IR of NiTPP[EAA]Br_6 (**1-Ni**) using KBr pellet at 298 K.

Figure S18. The IR of NiTPP[acac]Br_6 (**2-Ni**) using KBr pellet at 298 K.

Figure S19. The IR of CuTPP[EAA]Br_6 (**1-Cu**) using KBr pellet at 298 K.

Figure S20. The IR of CuTPP[acac]Br_6 (**2-Cu**) using KBr pellet at 298 K.

Figure S21. Comparative cyclic voltammogramms of NiTPP[EAA]Br_6 (**1-Ni**), CuTPP[EAA]Br_6 (**1-Cu**), and H_2TPP[EAA]Br_6 (**1-H_2**) in CH_2Cl_2 containing 0.1 M $TBAPF_6$ vs. Ag/AgCl as reference electrode at 298 K.

Figure S22. Comparative cyclic voltammogramms of NiTPP[acac]Br_6 (**2-Ni**), CuTPP[acac]Br_6 (**2-Cu**), and H_2TPP[acac]Br_6 (**2-H_2**) in CH_2Cl_2 containing 0.1 M $TBAPF_6$ vs. Ag/AgCl as reference electrode at 298 K.

Figure S23. Ground state optimized geometries of CuTPP[acac]Br_6 (**2-Cu**) and CuTPP[EAA]Br_6 (**1-Cu**) using B3LYP as functional set and LANL2DZ as the basis set. Left side: top view and right side: side view.

Figure S24. Ground state optimized geometries of NiTPP[acac]Br_6 (**2-Ni**) using B3LYP as functional set and LANL2DZ as the basis set. Left side: top view and right side: side view

Figure S25. Frontier molecular orbitals of CuTPP[EAA]Br_6 (**1-Cu**).

Figure S26. Frontier molecular orbitals of CuTPP[acac]Br_6 (**2-Cu**).

Figure S27. Frontier molecular orbitals of NiTPP[acac]Br_6 (**2-Ni**).

Figure S28. TD-DFT UV-vis Spectrum for H_2TPP[EAA]Br_6 (**1-H_2**) and H_2TPP[acac]Br_6 (**2-H_2**).

Figure S29. Optical NLO data under the excitation of femtosecond 1 kHz, 50 fs, 800 nm pulses. (a) Depicts open aperture data for Chloroform solvent. (b) Depicts closed aperture data for Chloroform solvent. 3d purple spheres exhibit the experimental data, whereas red line represents its corresponding theoretical fit.

Table S1. Photophysical data of synthesized porphyrins in $CHCl_3$ at 298 K.

Table S2. Data of selected bond angles (º) and bond lengths (Ǻ) calculated from ground state optimized geometries using B3LYP as functional and LANL2DZ as basis set.

EXPERIMENTAL SECTION

Materials

Copper(II) acetate monohydrate, nickel(II) acetate tetrahydrate, ethylacetoacetate, K_2CO_3, P_2O_5, CaH_2, acetylacetone, benzaldehyde, N-bromosuccinimde (NBS) and copper nitrate trihydrate were purchased from HiMedia, India and used as received except NBS. Pyrrole was purchased from Alfa Asear, UK. DMF, DMSO, and propionic acid were bought from Thomas Baker and utilized as obtained. The solvents ($CHCl_3$, hexane, dichloromethane, and methanol) employed in this work were of analytical grade and dried or distilled before use. NBS were recrystallized from hot water and dried in hot air oven for 7 hrs. DCM utilized for Cyclic voltammetric studies were distilled twice using P_2O_5 and finally with CaH_2. $TBAPF_6$ was

recrystallized in ethanol (hot) and dried for 24 h at 40 °C. Precoated silica chromatographic plates were purchased from E. Merck.

Instrumentation and methods employed

The optical electronic spectra were recorded on Shimadzu UV-2600 spectrophotometer using a pair of quartz cells with 1 cm × 1 cm dimension, 10 mm path length, and 3.5 ml volume in distilled chloroform. The steady-state emission spectra were recorded on Hitachi F-4600 spectrofluorometer using a quartz cell of 10 mm path length in distilled chloroform. The absolute quantum yield (ϕ) is determined by comparing the number of emitted photons with the number of absorbed photons using Edinburgh instruments FLS 980. All the proton and carbon NMR spectra were recorded on JEOL ECX400 MHz instrument in $CDCl_3$ (solvent) at 298 K. MALDI-TOF-MS were recorded in positive ion mode on BrukerUltrafleXtreme-TN MALDI-TOF/TOF spectrometer using HABA (2-(4-hydroxyphenylazo)benzoic acid) as a matrix at 298 K. The cyclic voltammetric studies were done on CH instruments (CHI 620E) by aid of a self-reliant three electrode assembly, comprising a working electrode (Platinum electrode), reference electrode (Ag/AgCl) and counter electrode (Platinum wire) using 0.1 M $TBAPF_6$ as supporting electrolyte at 298 K and 100 mV/s as scan rate. The electrochemical experiments were done in distilled CH_2Cl_2 with maintained concentration of approximately 1mM and degassing was done by purging argon gas. The optimization of synthesized porphyrins in ground state were done using Gaussian 16, where LANL2DZ was basis set and B3LYP as functional set. Elemental composition was measured using VarioMICRO CHNS instrument having serial number 15136064 using temperature range 1150 – 850 °C. Infrared red spectra were recorded PerkinElmer FTIR spectrometers. Using Lithium Tantalate MIR as detector with a SNR of 9300:1. The method employed for measurement was 2 mg chem80s.The NLO experiments were carried out by a femtosecond pulsed laser [M/s Coherent, Libra] with a pulse width ~50 fs, repetition rate of 1 kHz, and a wavelength of 800 nm. A lock-in amplifier and a photo-diode were utilized to gather the signals using LabVIEW program. We employed 1D translational stage to scan the sample within the Rayleigh range to collect NLO absorption and refraction data, more information is available in our earlier reports.[1-3]

Synthetic Procedures:

H_2TPP, CuTPP, NiTPP, CuTPP(NO_2), NiTPP(NO_2), CuTPP(NO_2)Br_6, and NiTPP(NO_2)Br_6 were synthesized according to literature methods.[4]

General Synthetic procedure of 2-(1-ethoxy-3-oxobutanone)-7,8,12,13,17,18-hexabromo-5,10,15,20-tetraphenyl Porphyrin/Porphyrinato metal (II); MTPP[EAA]Br_6 where M = 2H, Cu(II), Ni(II).

In a double neck R.B, 50 mg of MTPP(NO_2)Br_6 (M = 2H, Cu(II), and Ni(II)), 10 equiv. K_2CO_3, and 10 equiv. EAA (ethylacetoacetate) was added to 4 ml DMSO and the reaction mixture was degassed with argon gas for 15 minutes. After that, the reaction mixture was allowed to stir for 40 min at 60 °C on magnetic stirrer under inert conditions. After completion of the reaction, washing was given three times with saturated solution of sodium chloride and porphyrin was collected in chloroform, which was rota evaporated and resulted in crude product. The purification of crude product was done with the help of column chromatography using chloroform and hexane as eluent (3:2), further the recrystallization was done in $CHCl_3$:MeOH (2:98).

H_2TPP[EAA]Br_6 (1-H_2): Yield = 65%, 36 mg, 0.029 mmol, UV/Vis ($CHCl_3$): λ_{max}, nm (logε): 367(sh), 469(5.21), 566(4.93), 627(4.23), 741(3.88). ^{1}H NMR (400 MHz, $CDCl_3$) δ (ppm): 12.77(s,1H, -OH), 8.28(s,1H, *β*-H), 8.24-8.01(m, 8, meso-*o*-H), 7.91-7.60(m,12, meso-*m,p*-H),4.30-4.01(m, 2H, OCH_2), 2.17(s, 3H, $COCH_3$), 0.896-0.862(t, 3H, -CH_3), -1.69(bs, 2H, -NH). MALDI-TOF-MS (m/z): found $[M]^+$ = 1216.913, calcd. $[M]^+$ = 1216.255. Anal. Calcd. for $C_{50}H_{32}Br_6N_4O_3$: C, 49.38; H, 2.65; N, 4.61. Found C, 49.56; H, 2.28; N, 4.38.

CuTPP[EAA]Br6 (1-Cu): Yield = 72%, 38 mg, 0.0297 mmol, UV/Vis ($CHCl_3$): λ_{max}, nm (logε): 352 (sh), 442(4.74), 575(3.73), 622(3.27). MALDI-TOF-MS (m/z): found $[M^+ - Br]$ = 1197.768, calcd. $[M^+ - Br]$ = 1197.788. Anal. Calcd. for $C_{50}H_{30}Br_6CuN_4O_3$: C, 47.00; H, 2.37; N, 4.38. Found C, 46.25; H, 2.82; N, 4.92.

NiTPP[EAA]Br6 (1-Ni): Yield = 62%, 33 mg, 0.026 mmol, UV/Vis ($CHCl_3$): λ_{max}, nm (logε): 332 (sh), 441(5.19), 556(4.11), 598(3.76). ^{1}H NMR (400 MHz, $CDCl_3$) δ (ppm): 12.66(s,1H, -OH), 8.02(s,1H, *β*-H), 7.93-7.52(m,20, meso-*o,m,p*-H),4.22-3.94 (m, 2H, OCH_2), 2.34(s, 3H, $COCH_3$), 1.14-1.11(t, 3H, -CH_3). MALDI-TOF-MS (m/z): found $[M - COCH_3]^+$ = 1230.916, calcd. $[M - COCH_3]^+$ = 1230.916. Anal. Calcd. for $C_{50}H_{30}Br_6NiN_4O_3$: C, 47.18; H, 2.38; N, 4.40. Found C, 47.42; H, 2.06; N, 4.65.

General Synthetic procedure of 2-(1-Acetyl-2'-oxopropyl)-7,8,12,13,17,18-hexabromo-5,10,15,20-tetraphenyl Porphyrin/Porphyrinato metal (II); MTPP[acac]Br_6, where M = 2H, Cu(II), and Ni(II).

In a double neck R.B, 50 mg of MTPP(NO_2)Br_6 (M = 2H, Cu(II), and Ni(II)), 10 equiv. K_2CO_3, and 10 equiv. acac (acetylacetone) was added to 4 ml DMSO and purged with argon gas for 15 minutes. After purging, the reaction mixture was allowed to stir for 40 min at 60 °C on magnetic stirrer under inert conditions. After completion of the reaction, washing was given three times with saturated solution of sodium chloride, porphyrin was collected in chloroform, which was rota evaporated and resulted in crude product. The purification of crude product was done with the help of column chromatography using chloroform and hexane as eluent (3:2), further the recrystallization was done in $CHCl_3$:MeOH (2:98).

H_2TPP[acac]Br_6 (2-H_2): Yield = 69%, 36 mg,0.030 mmol, UV/Vis ($CHCl_3$): λ_{max}, nm (logε): 325(sh), 462(5.18), 560(3.92), 612(3.85),720(3.91). ^{1}H NMR (400 MHz, $CDCl_3$) δ (ppm): 16.44(s,1H, -OH), 8.27(s,1H, *β*-H), 8.23-7.97(m, 8, meso-*o*-H), 7.83-7.63 (m,12, meso-*m,p*-H), 2.163(s, 3H, -CH_3) . MALDI-TOF-MS (m/z): found $[M]^+$ = 1186.703, calcd. $[M]^+$ = 1186.229. Anal. Calcd. for $C_{49}H_{30}Br_6N_4O_2$: C, 49.61; H, 2.55; N, 4.72. Found C, 49.98; H, 2.82; N, 4.58.

CuTPP[acac]Br_6 (2-Cu): Yield = 80%, 42 mg, 0.033 mmol, UV/Vis ($CHCl_3$): λ_{max}, nm (logε): 354(sh), 443(5.23), 575(4.23), 626(3.74). MALDI-TOF-MS (m/z): found $[M]^+$ = 1247.981, calcd. $[M]^+$ = 1247.742. Anal. Calcd. for $C_{49}H_{28}Br_6CuN_4O_2$: C, 47.17; H, 2.26; N, 4.49. Found C, 47.34; H, 2.02; N, 4.18.

NiTPP[acac]Br_6 (2-Ni): Yield = 59%, 31 mg, 0.025 mmol, UV/Vis ($CHCl_3$): λ_{max}, nm (logε): 333(sh), 443(5.09), 558(3.98), 593(3.66). ^{1}H NMR (400 MHz, $CDCl_3$) δ (ppm): 16.33(s,1H, -OH), 8.06(s,1H, *β*-H), 7.96-7.92(m, 6, meso-*o*-H), 7.74-7.55 (m,14, meso-*m,p*-H), 1.810(s, 3H, -CH_3). MALDI-TOF-MS (m/z): found $[M+H]^+$ = 1243.901, calcd. $[M+H]^+$ = 1243.902. Anal. Calcd. for $C_{49}H_{28}Br_6NiN_4O_2$: C, 47.35; H, 2.27; N, 4.51. Found C, 47.51; H, 2.32; N, 4.29.

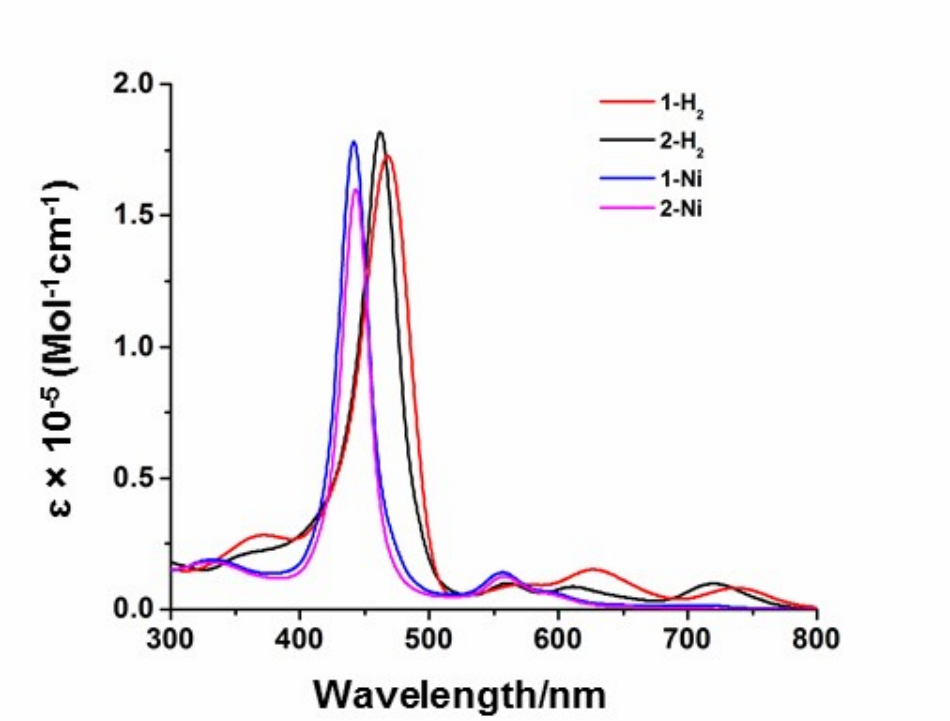

Figure S1. The optical absorption spectra of H_2TPP[EAA]Br_6 (**1-H_2**), H_2TPP[acac]Br_6 (**2-H_2**), NiTPP[EAA]Br_6 (**1-Ni**), and NiTPP[acac]Br_6 (**2-Ni**) in $CHCl_3$ at 298 K.

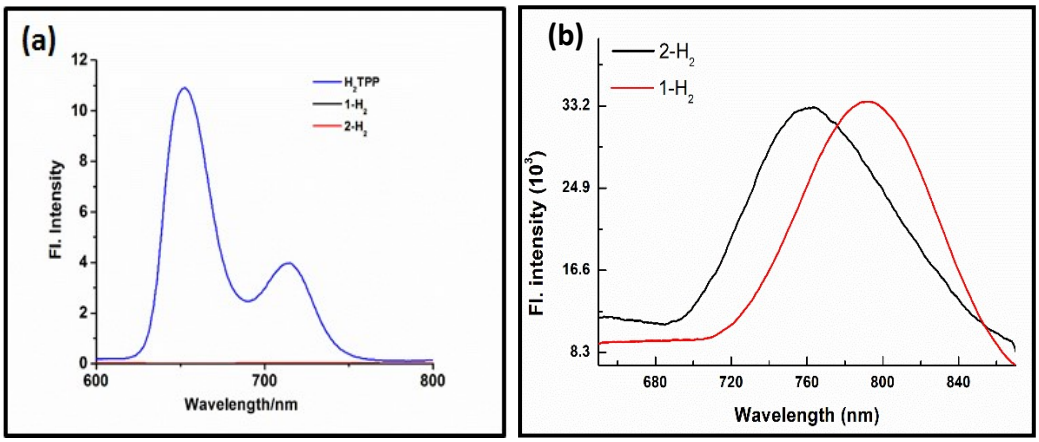

Figure S2. (a) The comparative emission spectra of H_2TPP, H_2TPP[EAA]Br_6 (**1-H_2**), and H_2-TPP[acac]Br_6 (**2-H_2**) in $CHCl_3$ at 298 K. (b) The emission spectra of H_2TPP[EAA]Br_6 (**1-H_2**), and H_2-TPP[acac]Br_6 (**2-H_2**) in $CHCl_3$ at 298 K.

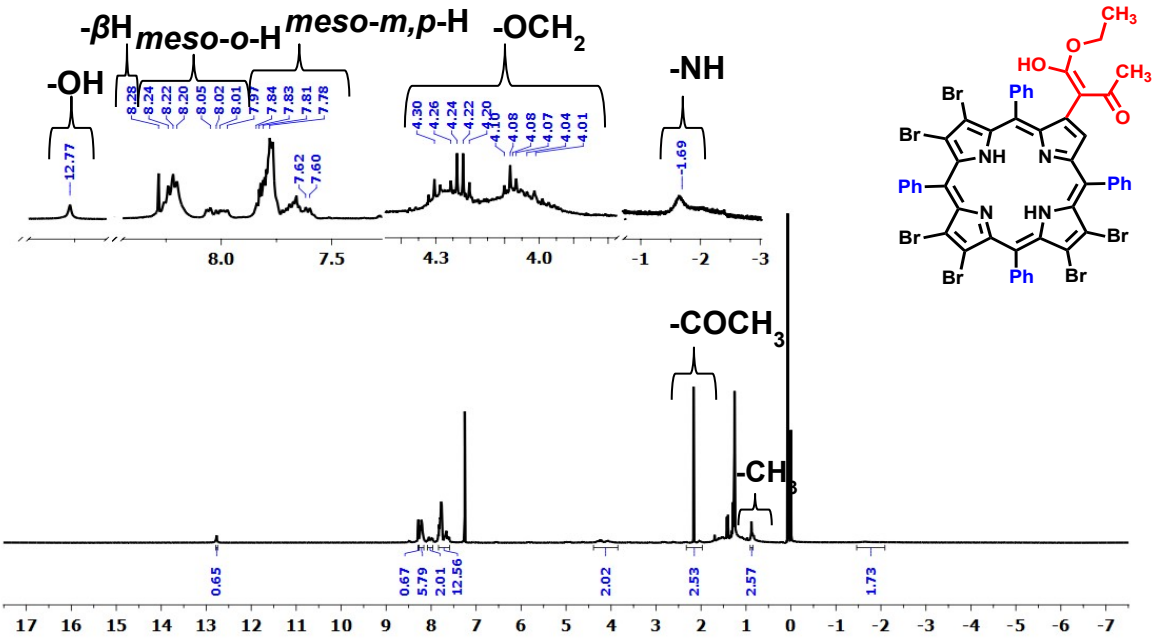

Figure S3. The ^{1}H NMR spectrum of H_2TPP[EAA]Br_6 (**1- H_2**) in $CDCl_3$ at 298 K.

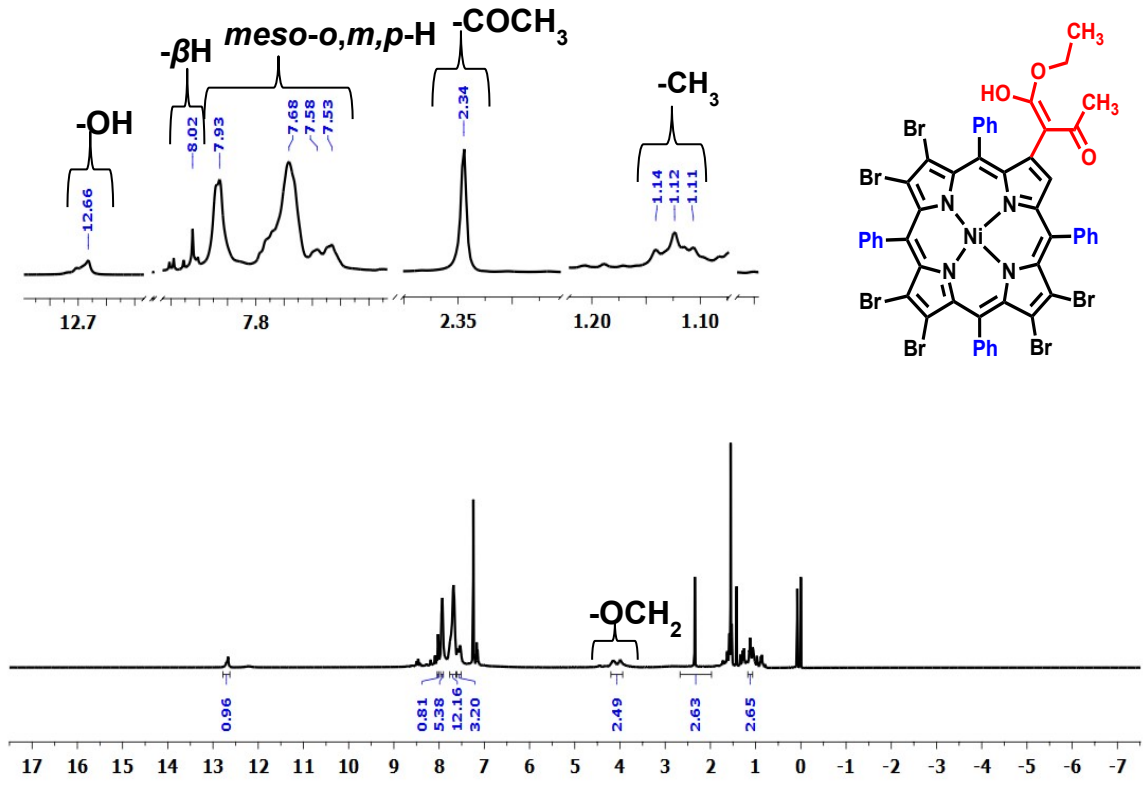

Figure S4. The ^{1}H NMR spectrum of NiTPP[EAA]Br6 (**1-Ni**) in $CDCl_3$ at 298 K.

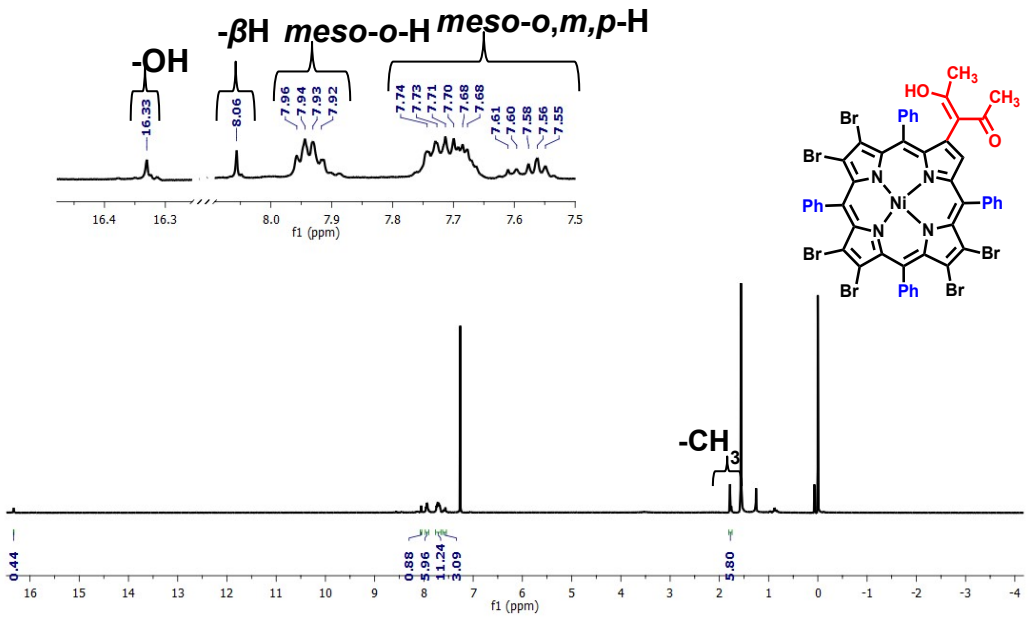

Figure S5. The ^{1}H NMR spectrum of NiTPP[acac]Br_6 (**2-Ni**) in $CDCl_3$ at 298 K.

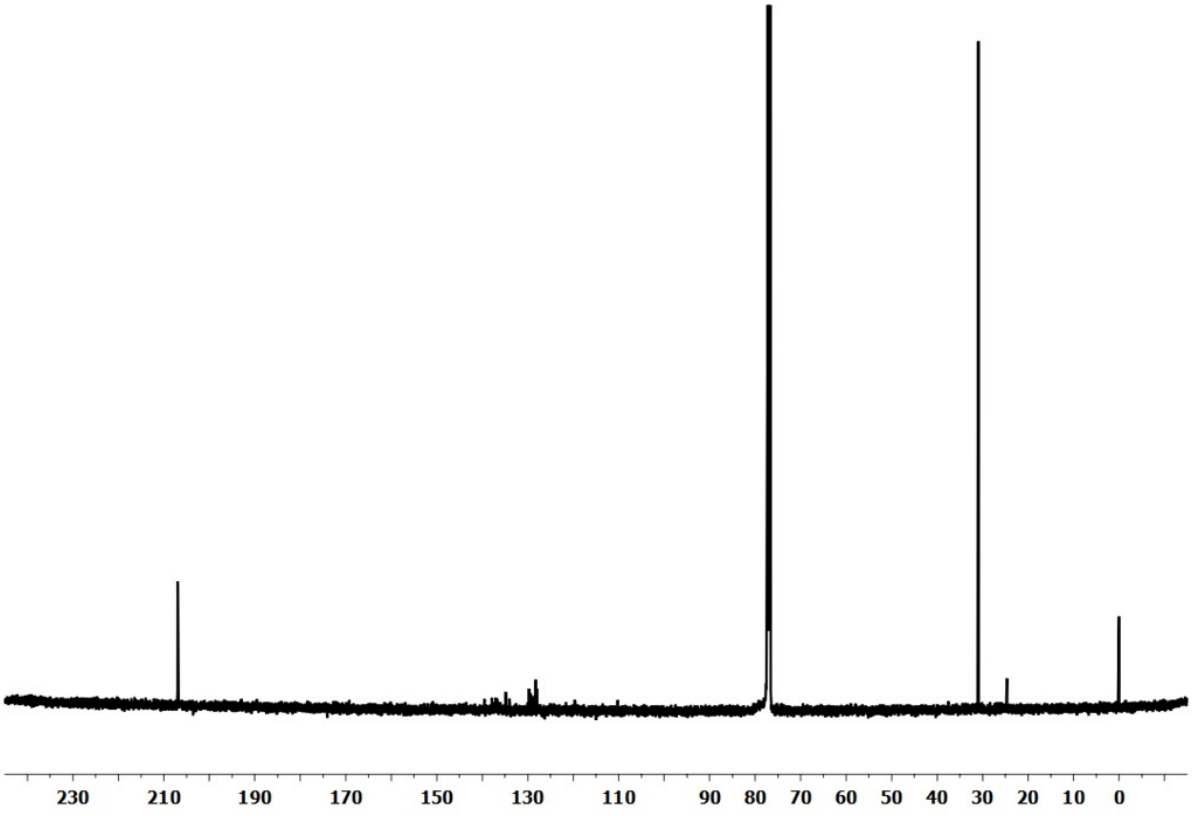

Figure S6. The ^{13} C NMR spectrum of H_2TPP[EAA]Br_6 (**1-H_2**) in $CDCl_3$ at 298 K.

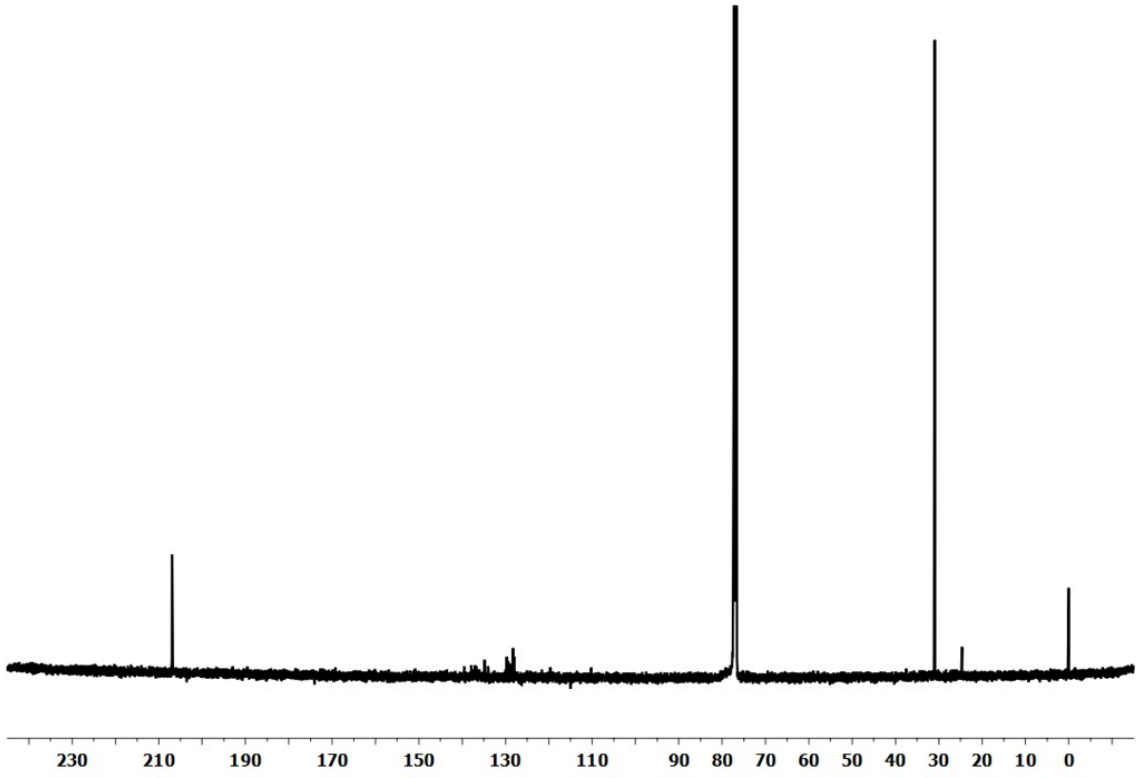

Figure S7. The ^{13} C NMR spectrum of H_2TPP[acac]Br_6 (**2-H_2**) in $CDCl_3$ at 298 K.

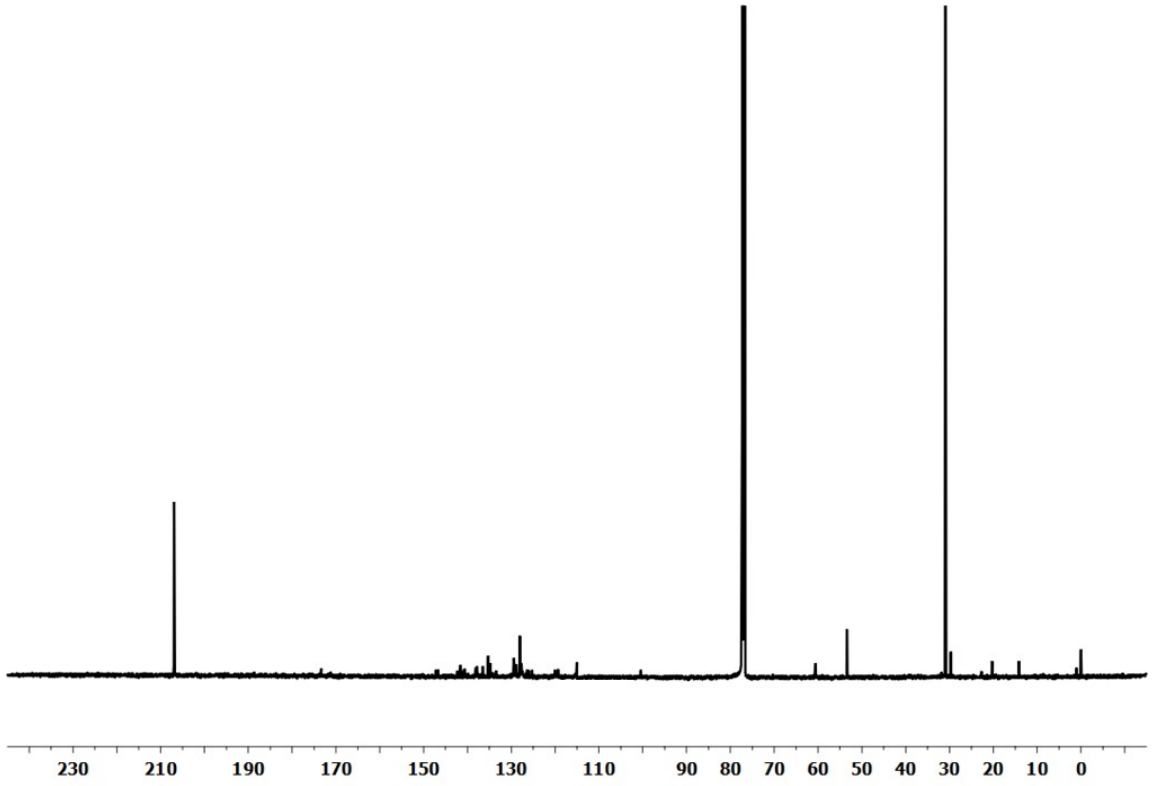

Figure S8. The ^{13} C NMR spectrum of NiTPP[EAA]Br_6 (**1-Ni**) in $CDCl_3$ at 298 K.

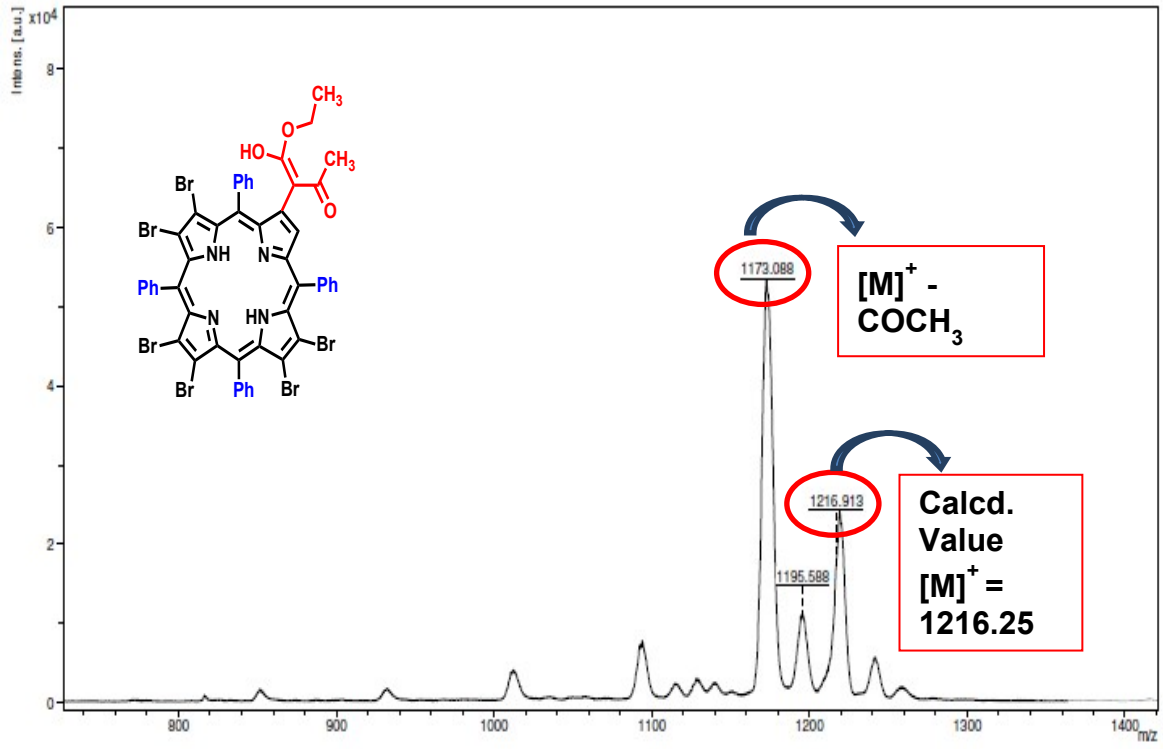

Figure S9. The MALDI-TOF-MS of H_2TPP[EAA]Br_6 (**1-H$_2$**) in positive ion mode using HABA as matrix at 298 K.

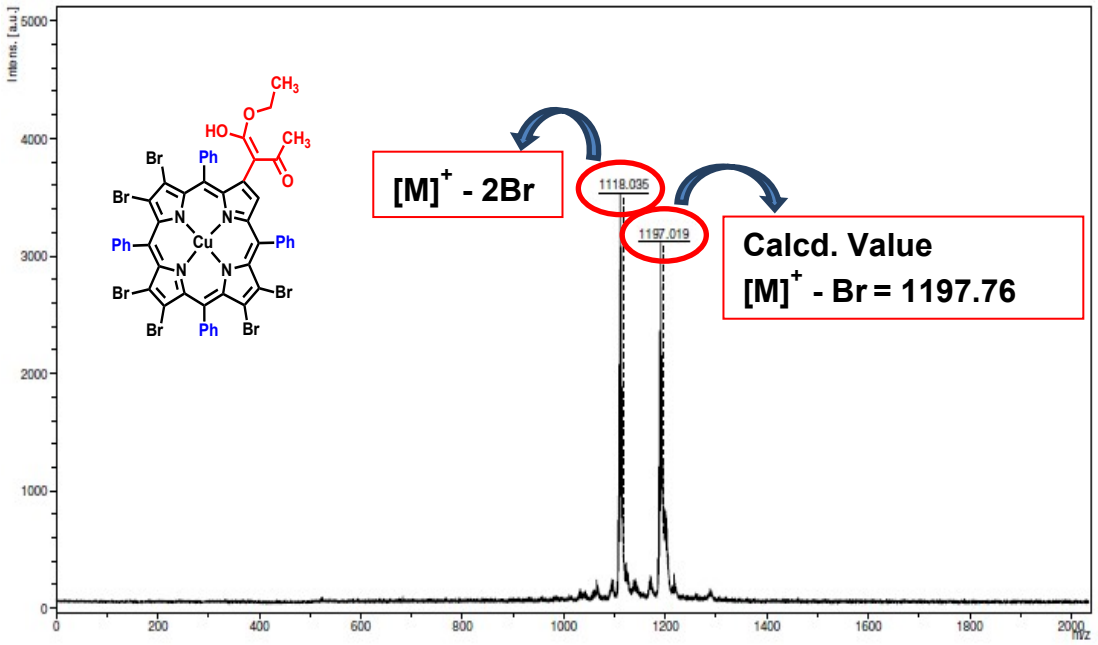

Figure S10. The MALDI-TOF-MS of CuTPP[EAA]Br_6 (**1-Cu**) in positive ion mode using HABA as matrix at 298 K.

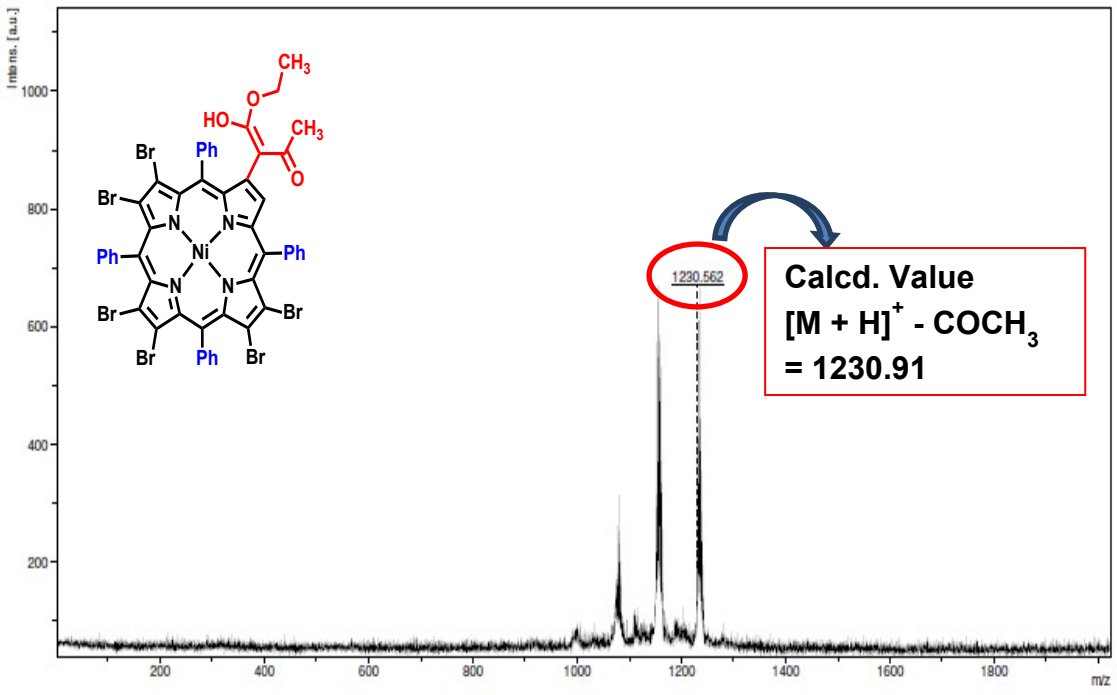

Figure S11. The MALDI-TOF-MS of NiTPP[EAA]Br_6 (**1-Ni**) in positive ion mode using HABA as matrix at 298 K.

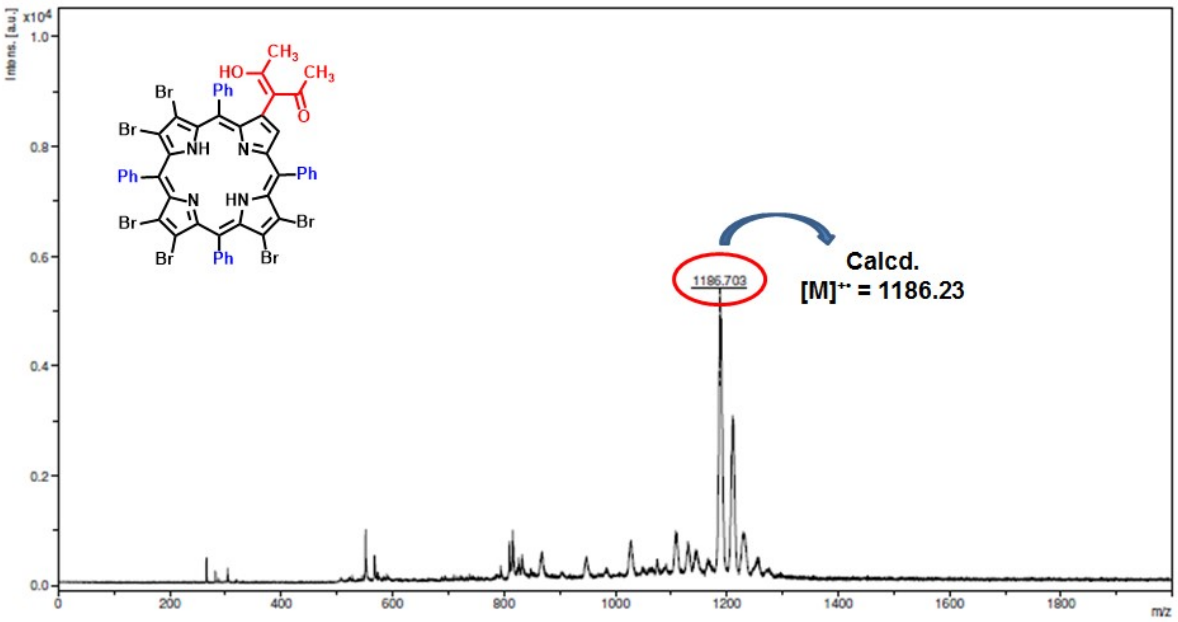

Figure S12. The MALDI-TOF-MS of H_2TPP[acac]Br_6 (**2-H_2**) in positive ion mode using HABA as matrix at 298 K.

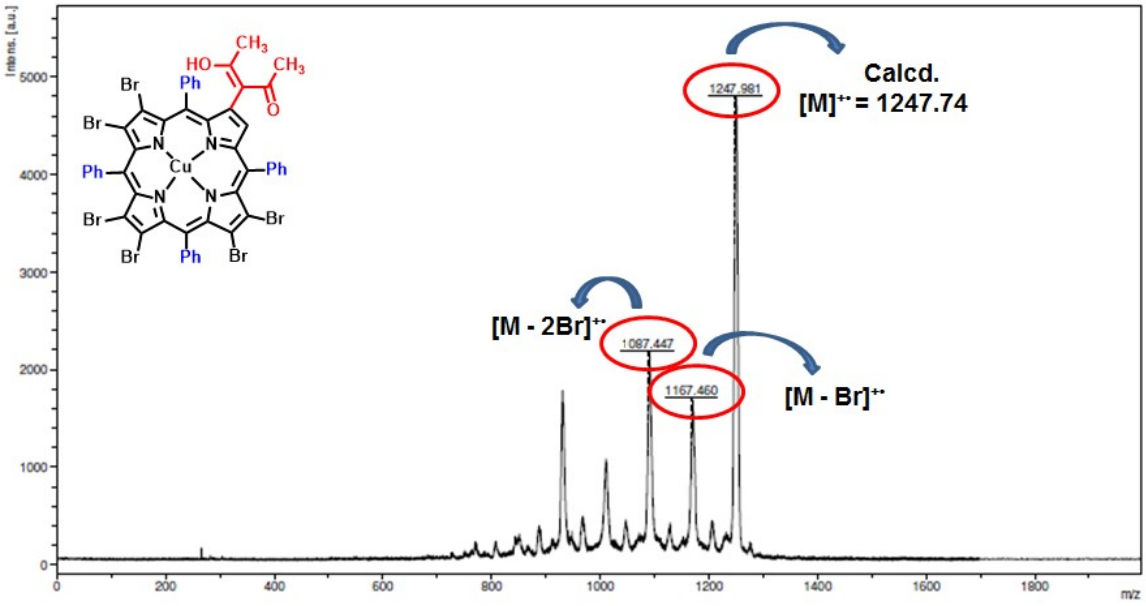

Figure S13. The MALDI-TOF-MS of CuTPP[acac]Br_6 (**2-Cu**) in positive ion mode using HABA as matrix at 298 K.

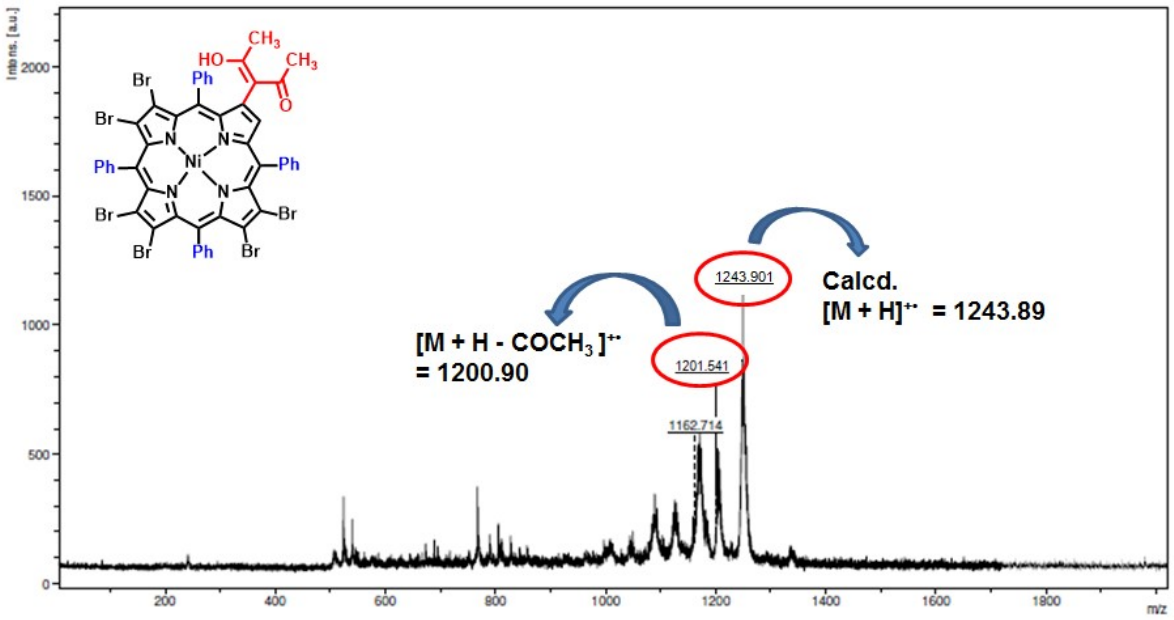

Figure S14. The MALDI-TOF-MS of NiTPP[acac]Br_6 (**2-Ni**) in positive ion mode using HABA as matrix at 298 K.

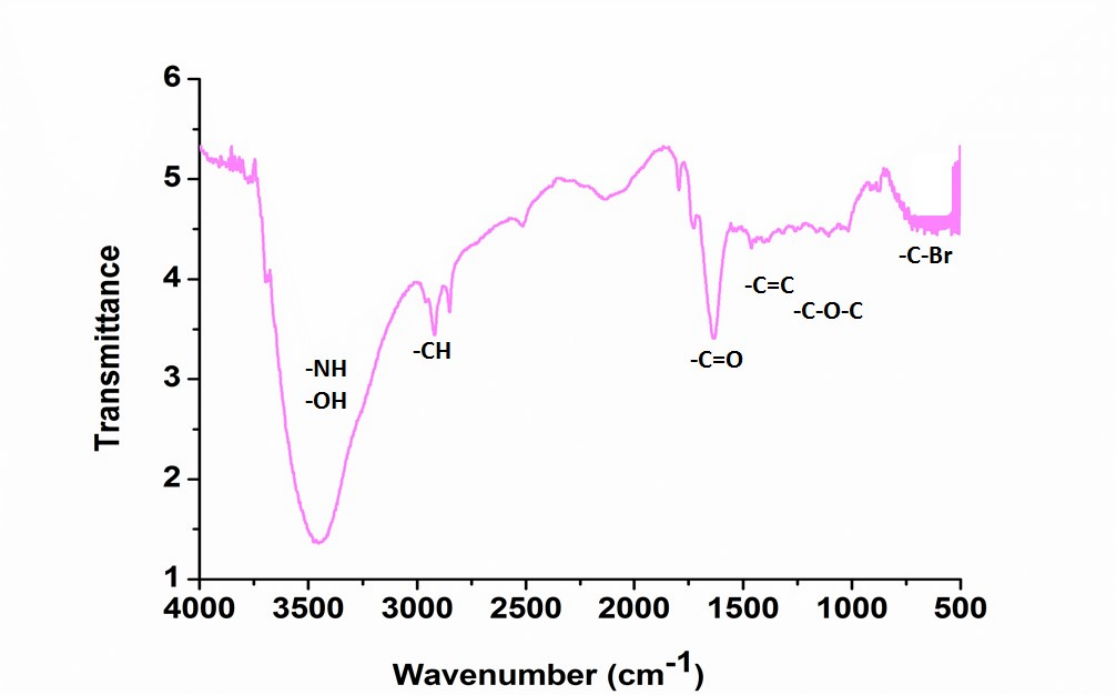

Figure S15. The IR of H_2TPP[EAA]Br_6 (**1-H_2**) using KBr pellet at 298 K.

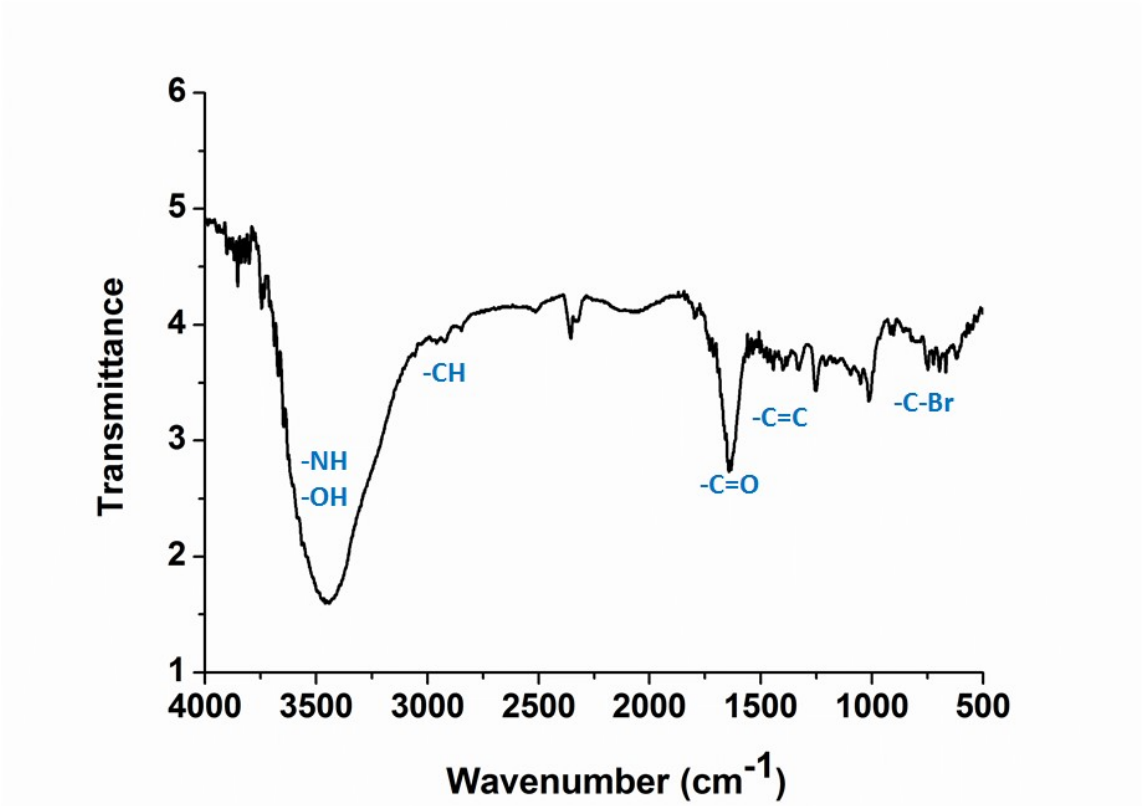

Figure S16. The IR of H_2TPP[acac]Br_6 (**2-H_2**) using KBr pellet at 298 K.

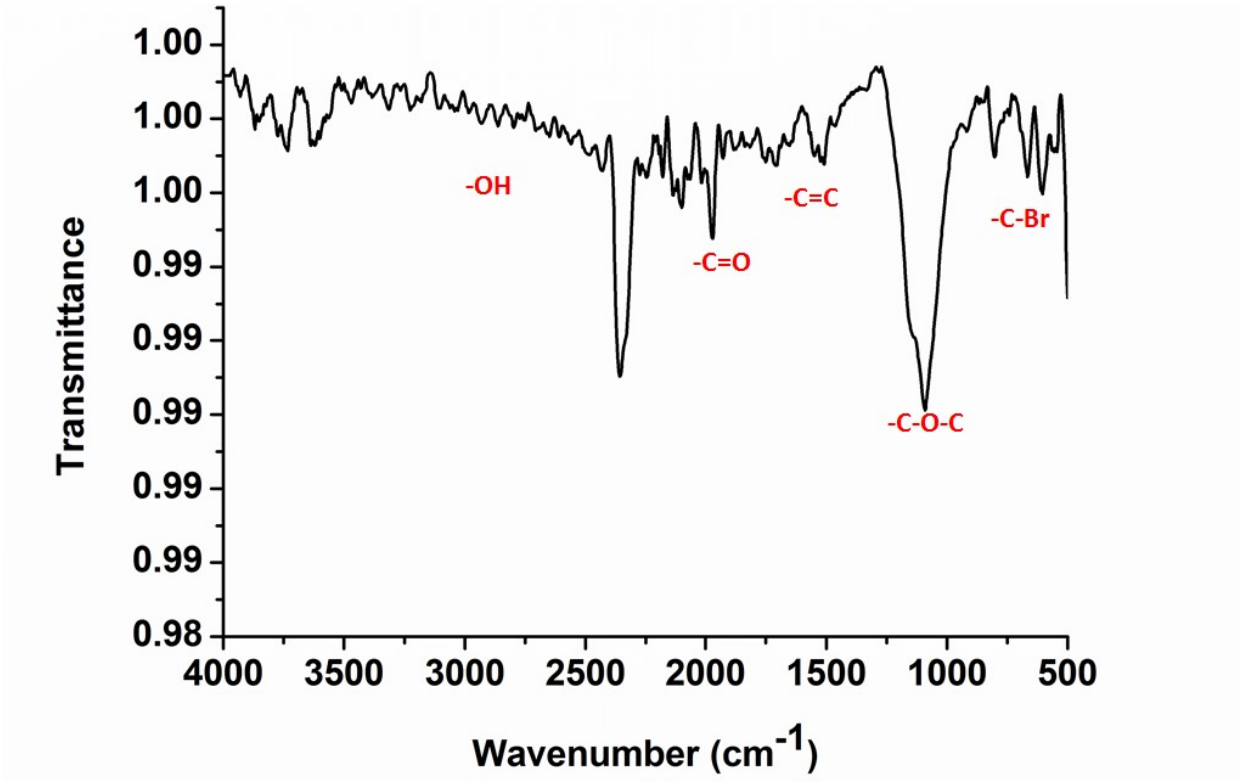

Figure S17. The IR of NiTPP[EAA]Br_6 (**1-Ni**) using KBr pellet at 298 K.

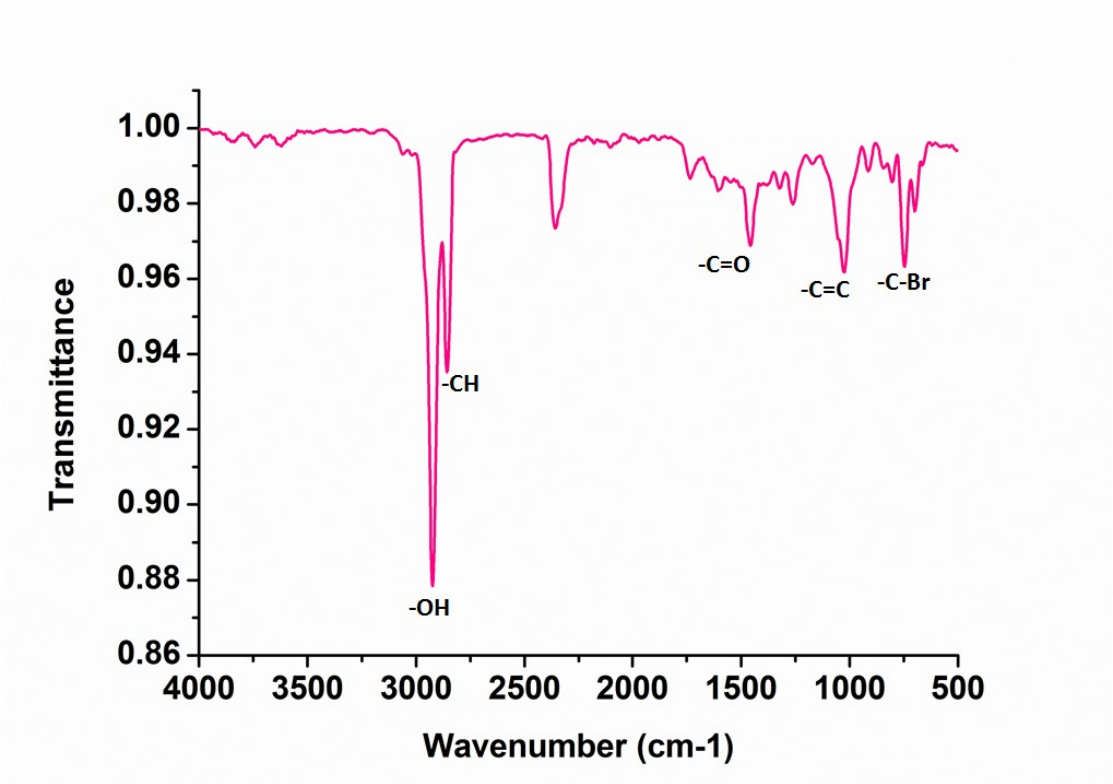

Figure S18. The IR of NiTPP[acac]Br_6 (**2-H_2**) using KBr pellet at 298 K.

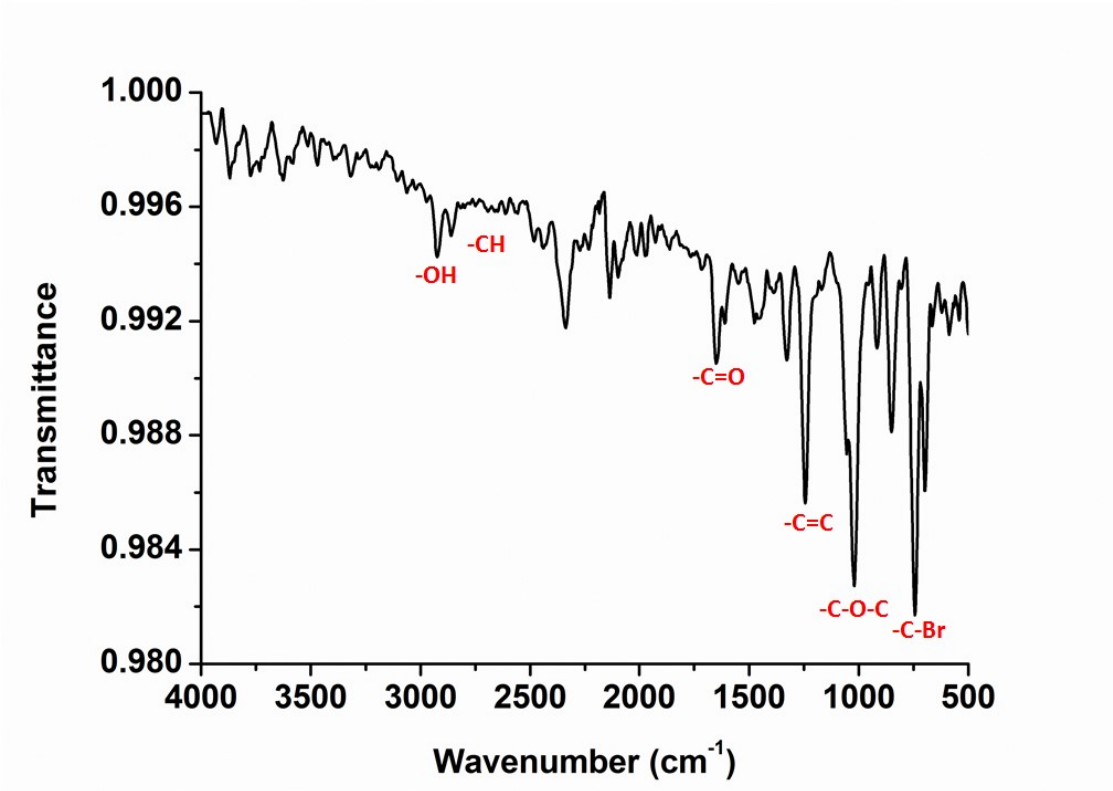

Figure S19. The IR of CuTPP[EAA]Br_6 (**1-Cu**) using KBr pellet at 298 K.

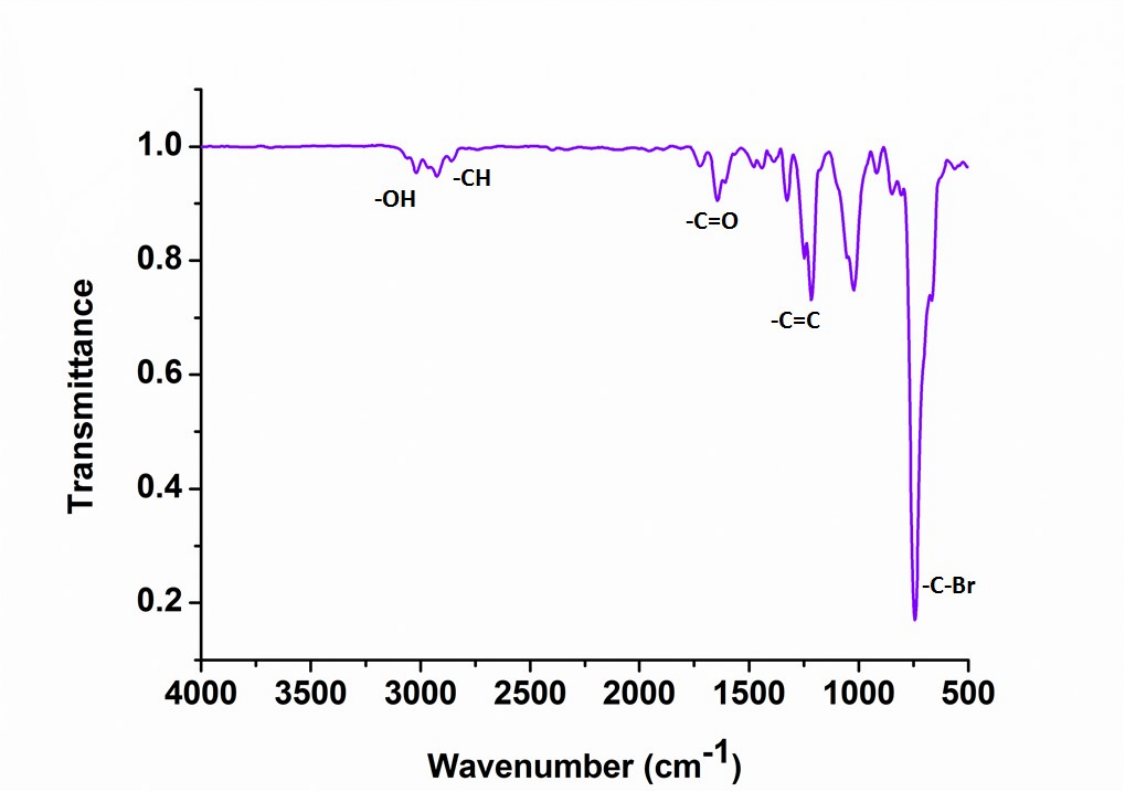

Figure S20. The IR of CuTPP[acac]Br_6 (**2-Cu**) using KBr pellet at 298 K.

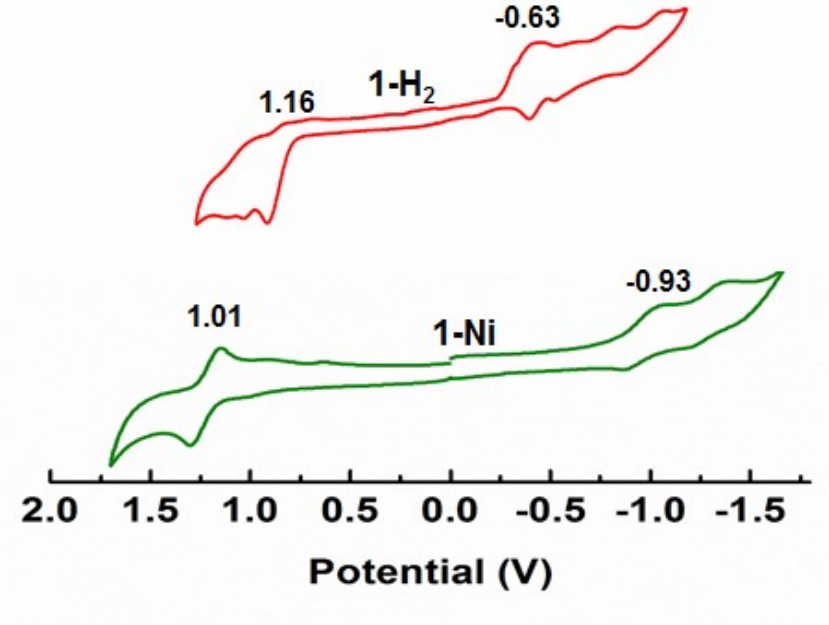

Figure S21. Comparative cyclic voltammogramms of NiTPP[EAA]Br_6 (**1-Ni**), and H_2TPP[EAA]Br_6 (**1-H_2**) in CH_2Cl_2 containing 0.1 M $TBAPF_6$ vs. Ag/AgCl as reference electrode at 298 K.

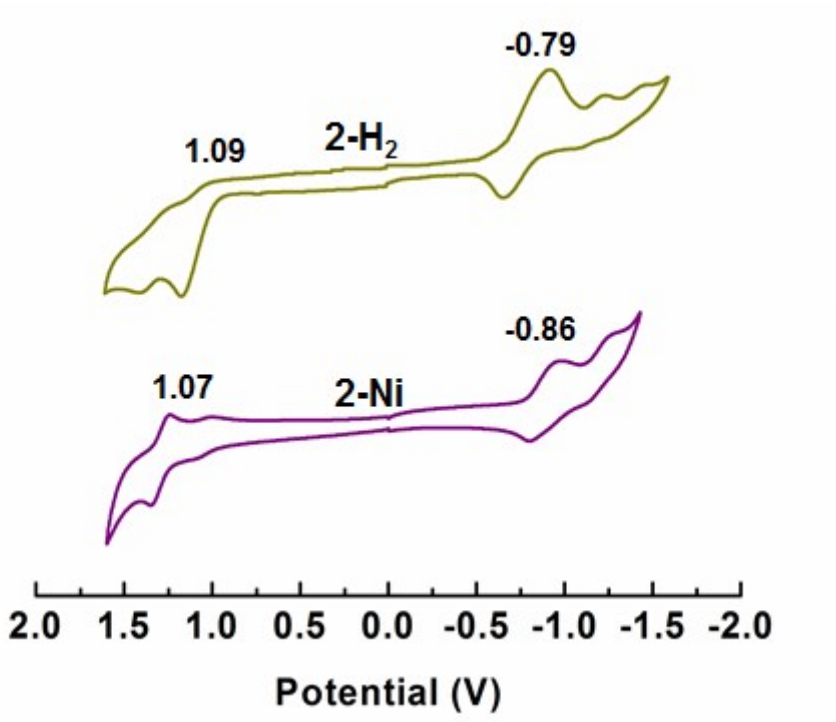

Figure S22. Comparative cyclic voltammogramms of $NiTPP[acac]Br_6$ (**2-Ni**), and $H_2TPP[acac]Br_6$ (**2-H_2**) in CH_2Cl_2 containing 0.1 M $TBAPF_6$ vs. Ag/AgCl as reference electrode at 298 K.

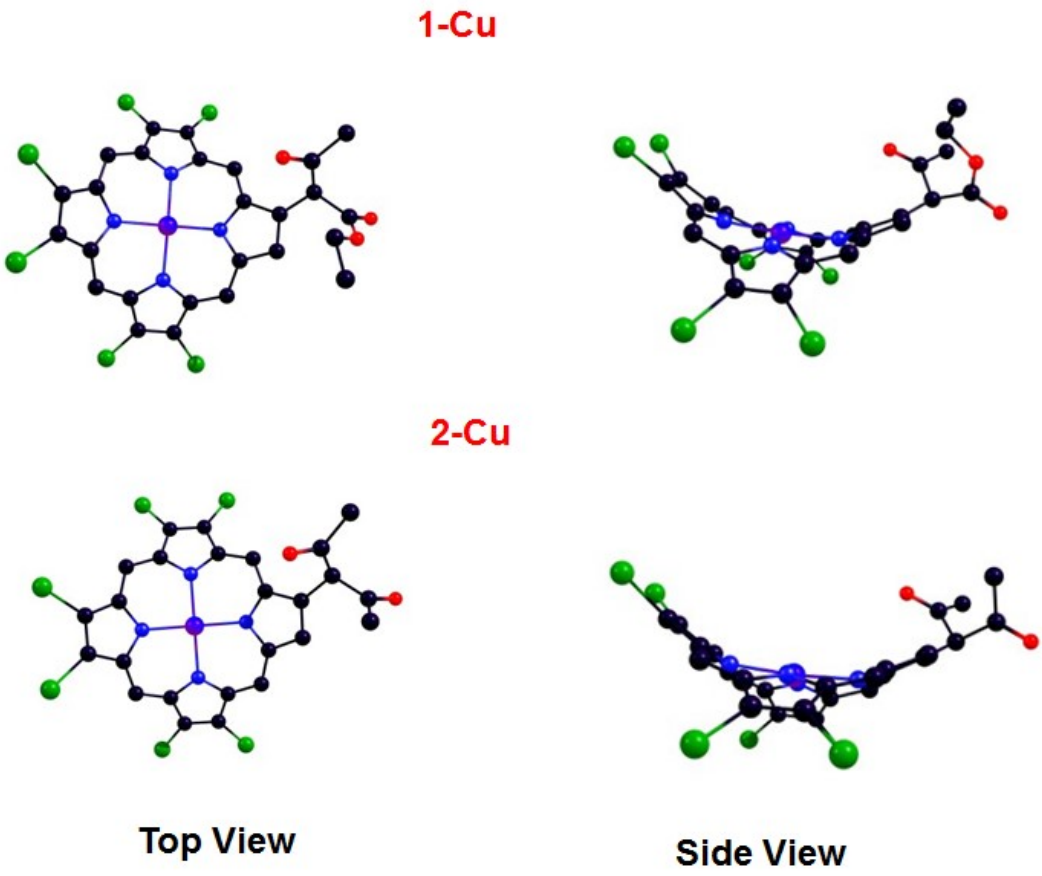

Figure S23. Ground state optimized geometries of CuTPP[EAA]Br_6 (**1-Cu**) and CuTPP[acac]Br_6 (**2-Cu**) using B3LYP as functional set and LANL2DZ as the basis set. Left side: top view and right side: side view.

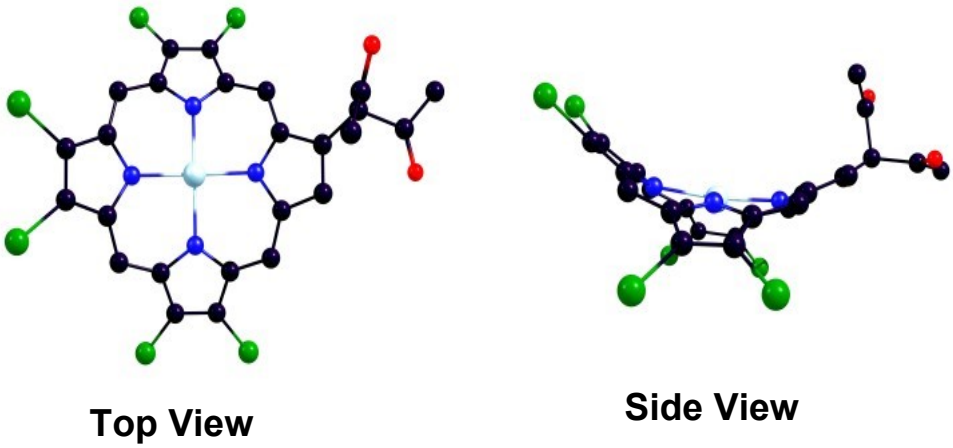

Figure S24. Ground state optimized geometry of NiTPP[acac]Br_6 (**2-Ni**) using B3LYP as functional set and LANL2DZ as the basis set. Left side: top view and right side: side view.

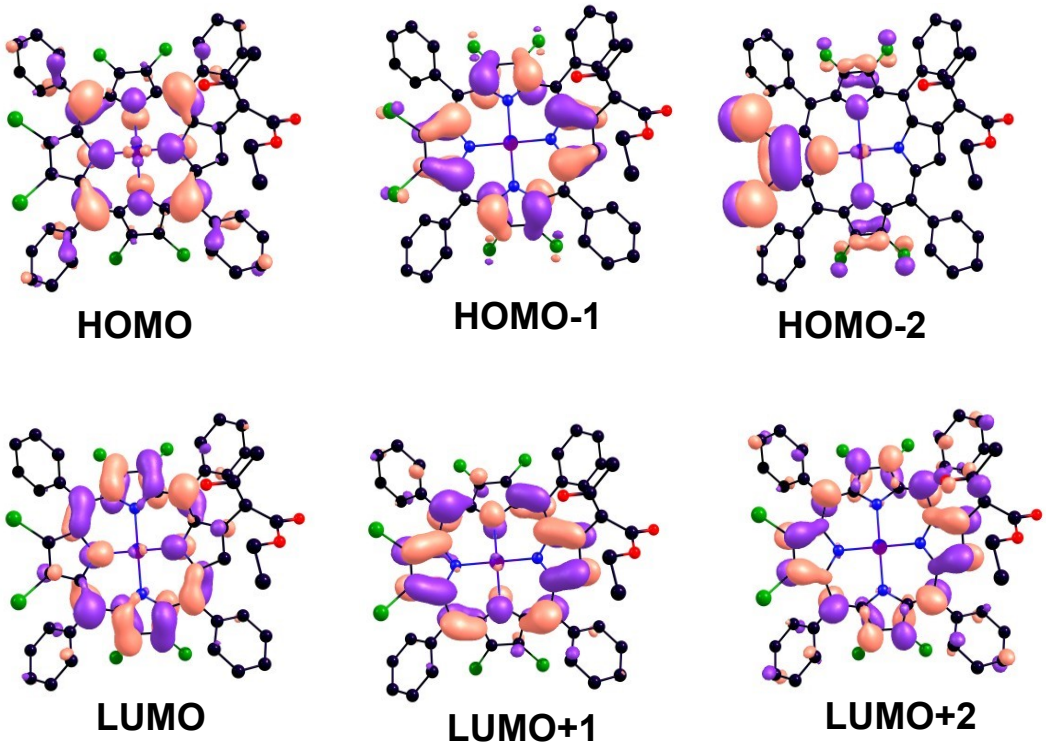

Figure S25. Frontier molecular orbitals of CuTPP[EAA]Br_6 (**1-Cu**).

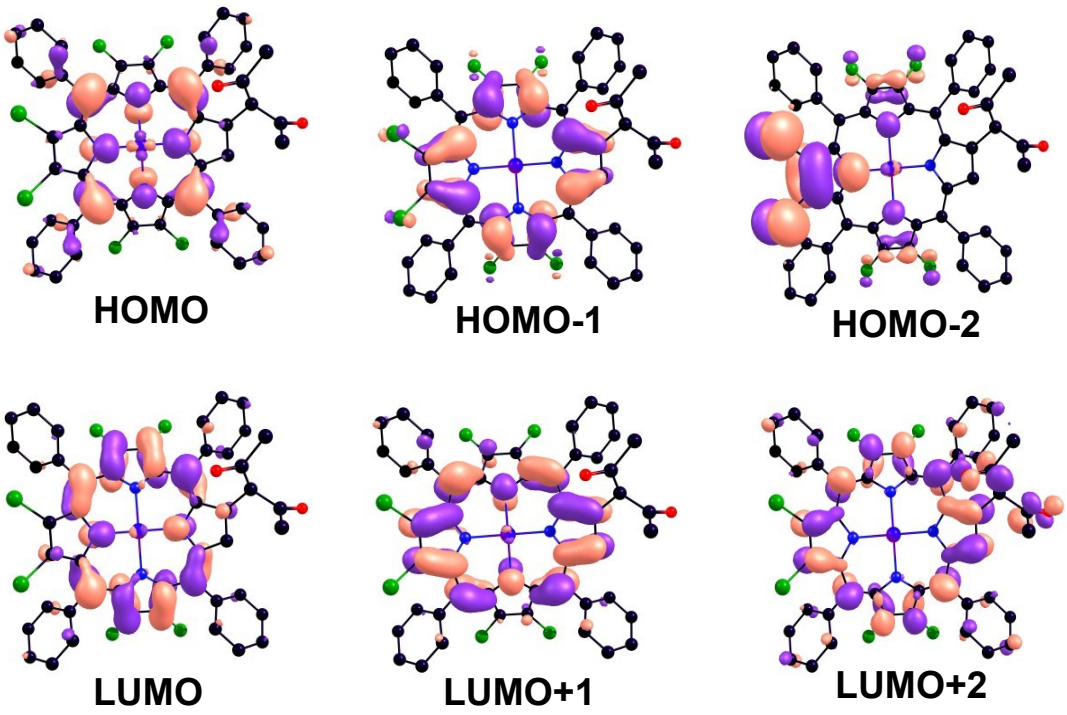

Figure S26. Frontier molecular orbitals of CuTPP[acac]Br_6 (**2-Cu**).

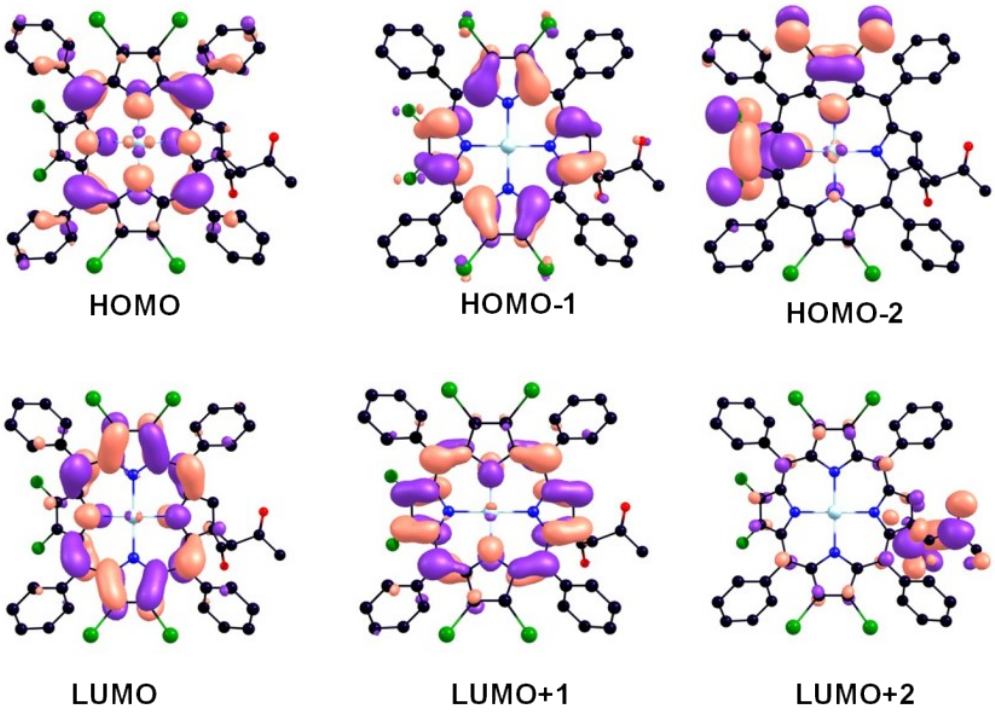

Figure S27. Frontier molecular orbitals of NiTPP[acac]Br_6 (**2-Ni**).

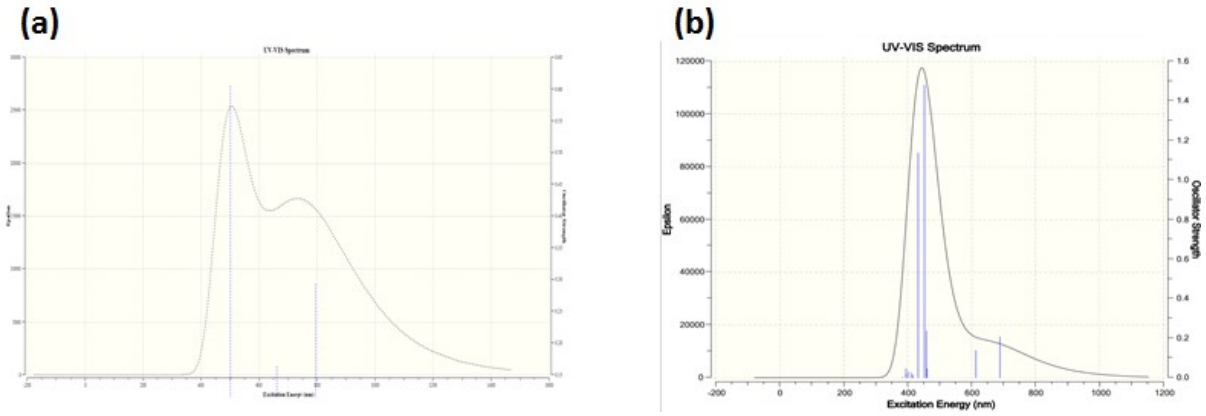

Figure S28. TD-DFT UV-vis Spectrum for H_2TPP[EAA]Br_6 (**1-H_2**) and H_2TPP[acac]Br_6 (**2-H_2**) respectively.

Table S1. The photophysical data of synthesized porphyrins in $CHCl_3$ at 298 K.

Porphyrins	λ_{abs} (nm)		λ_{em} (nm)	ϕ_f
	B-band	**Q-bands**		
H_2TPP[EAA]Br_6 (1-H_2)	367(sh), 469(5.21)	566(3.93), 627(4.13), 741(3.88)	742	0.0093
CuTPP[EAA]Br_6 (1-Cu)	352(sh), 442(4.73)	575(3.73), 622(3.28)		
NiTPP[EAA]Br_6 (1-Ni)	332(sh), 441(5.19)	556(4.11), 598(3.75)		
H_2TPP[acac]Br_6 (2-H_2)	325(sh), 462(5.18)	560(3.92), 612(3.85), 720(3.91)	709	0.012
CuTPP[acac]Br_6 (2-Cu)	354(sh), 443(5.23)	575(4.23), 626(3.74)		
NiTPP[acac]Br_6 (2-Ni)	332(sh), 441(5.09)	556(3.98), 598(3.66)		

* Within parenthesis is logε

Table S2. Data of selected bond angles (º) and bond lengths (Å) of H_2TPP[EAA]Br_6 (**1-H_2**), H_2TPP[acac]Br_6 (**2-H_2**), CuTPP[EAA]Br6 (**1-Cu**), CuTPP[acac]Br_6 (**2-Cu**), and NiTPP[acac]Br_6 (**2-Ni**), calculated from ground state optimized geometries using B3LYP as functional and LANL2DZ as basis set.

	H_2TPP[EAA]Br_6 (**1-H_2**)	H_2TPP[acac]Br_6 (**2-H_2**)	CuTPP[EAABr_6 (**1-Cu**)	CuTPP[acac]Br_6 (**2-Cu**)	NiTPP[acac]Br_6 (**2-Ni**)
Bond length (Å)					
M - N	--	--	2.003	2.004	2.013
M - N′	--	--	2.016	2.015	2.025
N- C_α	1.391	1.390	1.395	1.392	1.394
N - C_α′	1.387	1.387	1.396	1.396	1.397
C_α - C_β	1.446	1.450	1.460	1.460	1.462
C_α′ - C_β′	1.470	1.473	1.459	1.459	1.460
C_β - C_β	1.391	1.388	1.379	1.379	1.380
C_β′ - C_β′	1.379	1.377	1.381	1.381	1.381
C_α - C_m	1.422	1.418	1.415	1.415	1.417
C_α′ - C_m	1.429	1.425	1.416	1.417	1.418
Δ24	0.546	0.546	0.559	0.558	0.545
ΔC_β	0.973	1.160	1.161	1.62	1.112
ΔM			0.006	0.014	0.000
Bond Angle (°)					

N - M - N	--	--	173.67	174.07	172.58
N′ - M - N′	--	--	173.17	172.87	173.06
M - N - C_α	--	--	123.65	123.60	124.17
M - N′ - C_α'	--	--	123.47	123.46	123.79
N - C_α - C_m	124.07	124.37	123.58	123.54	123.73
N′ - C_α' - C_m	122.64	123.09	123.08	123.08	123.33
N - C_α - C_β	105.75	105.54	108.39	108.40	108.31
N′ - C_α' - C_β'	109.05	108.95	108.00	108.01	107.82
C_β - C_α - C_m	129.59	129.91	127.77	127.79	127.73
C_β'- C_α' - C_m	127.92	127.73	128.64	128.62	128.60
C_α - C_m- C_α'	120.95	122.35	121.35	121.34	122.07
C_α - N- C_α	111.67	111.83	107.74	107.74	107.85
C_α' - N- C_α'	107.48	107.54	108.16	108.16	108.37

Δ24 = displacement for porphyrin core atoms from mean plane, ΔC_β = mean plane displacement of *β* pyrrole

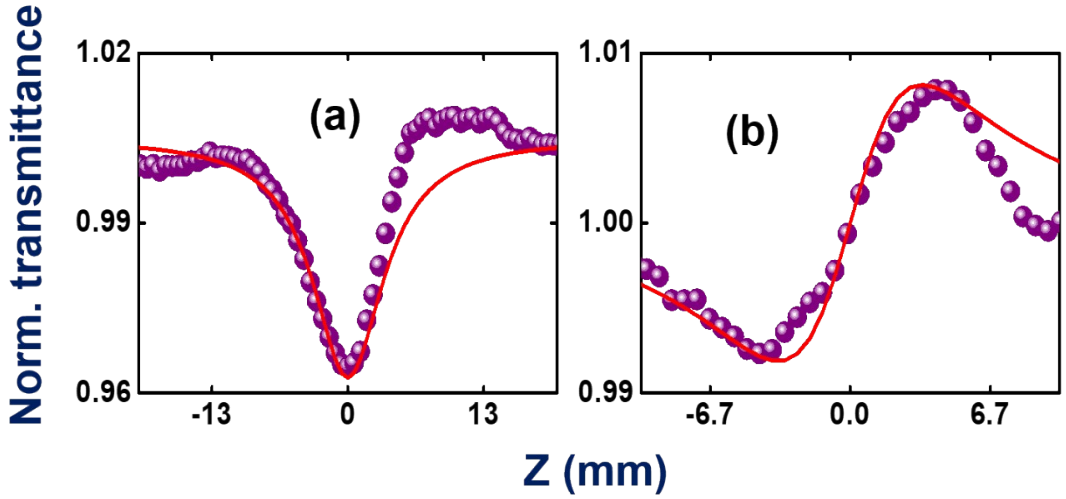

carbon atoms.

Figure S29. Optical NLO data under the excitation of femtosecond 1 kHz, 50 fs, 800 nm pulses. (a) Depicts open aperture data for Chloroform solvent. (b) Depicts closed aperture data for Chloroform solvent. 3d purple spheres exhibit the experimental data, whereas red line represents its corresponding theoretical fit.

References:

1. D. Banerjee, S. S. B. Moram, C. Byram, J. Rathod, T. Jena, G. K. Podagatlapalli and S. V. Rao, *Appl. Surf. Sci.*, 2021, **569** , 151070.
2. K. S. Srivishnu, D. Banerjee, R. A. Ramnagar, J. Rathod, L. Giribabu and S. V. Rao, *Front. Chem.*, 2021, **9**, 1–14.
3. C. Biswas, S. G. Palivela, L. Giribabu, S. V. Rao and S. S. K. Raavi, *Opt. Mater.*, 2022, **127**, 112232.

4. R. Kumar and M. Sankar, *Inorg. Chem.* 2014, **53**,12706-12719.